Structural Importance of Stone-Thrower-Wales Defects in Rolled and Flat Graphenes from Surface-Enhanced Raman Scattering

T. Fujimori [a], Ljubisa R. Radovic [b,c], Alejandro B. Silva-Tapia [c], M. Endo [a], K. Kaneko [a,*]

[a]Research Center for Exotic Nanocarbons (JST), Shinshu University, 4-17-1 Wakasato, Nagano-city 380-8553, Japan

[b]The Pennsylvania State University, Department of Energy and Mineral Engineering, University Park, PA 16802, USA

[c]University of Concepción, Department of Chemical Engineering, Concepción, Chile

*Corresponding author: TEL: +81 26 269 5743. Fax: +81 26 269 5737.

E-mail address: kkaneko@shinshu-u.ac.jp (K. Kaneko)

[ABSTRACT]

We first survey the historical aspects of the term Stone-Thrower-Wales (STW) defect and its experimental identification. Physicochemical properties associated with the STW defect have been extensively investigated theoretically as well. However, it is difficult to verify the predicted properties by means of experiments. Here we demonstrate an experimental way to probe the vibrational properties of STW defects in single-wall carbon nanotubes (SWCNTs) using surface-enhanced Raman scattering (SERS). We

also performed density functional theory calculations to support our interpretation of the SERS spectra. The characteristic fluctuations of peak intensities and frequencies are ascribed to dynamic motion of a STW defect in the hexagonal SWCNT lattice. The role of a STW defect at edges is also discussed in terms of its relevance to the stability and O_2 reactivity of flat and curved graphene structures.

[Body]

1. Introduction

The presence of topological defects, which are non-hexagonal arrangements of carbon atoms incorporated in the graphene lattice, provides unique and diverse morphologies to graphene-based materials (e.g., single-wall carbon nanotube (SWCNT)). Curved geometries have been theoretically explained by the presence of topological defects in carbon materials [1-3] since the discovery of fullerenes [4]. Not only a trapped pentagon, which is the key constituent of fullerenes, but a heptagon and even higher polygons are candidates for interpreting the wide variety of curved carbon nanostructures [5-7]. Indeed, attractive carbon nanostructures are derived theoretically by introducing such topological defects. For example, a seamless junction of two different chiralities of carbon nanotubes can be constructed by introducing one pentagon-heptagon pair at the junction; this offers exciting opportunities for novel

applications of nano-scale electronic devices.

Since the pentagon and heptagon induce positive and negative curvature in the hexagonal network, respectively, a pentagon-heptagon pair does not introduce net curvature and the planar structure is preserved. This has been shown in a pioneering study by Thrower [8] in the context of dislocation defects produced by graphite irradiation. A configuration with two pentagon-heptagon pairs is now called the Stone-Thrower-Wales (STW) defect [8,9], as discussed in detail below. Recent progress in experimental techniques has allowed us to perceive directly such defects by means of high-resolution transmission electron microscopy (HR-TEM) [10,11]. Experimental evidence in turn helps to further develop defect-associated science and provide new insight into the physical and chemical properties of carbon materials. Electronic, optical and mechanical properties, as well as chemical reactivity related to the STW defect have been extensively studied, mainly by theoretical methods [12-15]. However, further experimental evidence is needed to elucidate these effects and this has not been possible, presumably because of low concentrations of such defects.

In this context, ultrasensitive techniques are required to unveil properties associated with the presence of STW defects. Since the Raman cross-section can be strongly enhanced when matter is located in close vicinity of metal nanostructures (e.g., silver or

gold nanoparticles) - a phenomenon called surface-enhanced Raman scattering (SERS) [16] - the SERS technique is a promising tool for probing atomic vibrations due to very few topological defects in the hexagonal lattice.

Here we first provide a brief historical and conceptual account of the STW defect. We then focus on the STW defect-associated vibrational properties in a SWCNT as revealed by the SERS technique. Assignments for the SERS spectra are supported by vibrational frequency calculations using density functional theory (DFT). How the presence of a STW defect affects the chemical reactivity of flat and rolled graphene is also analyzed.

2. STW defect and related topological defects

2.1 The contribution of P. A. Thrower

The presence of a pentagon-heptagon pair (5-7 pair) in the basal plane of neutron-irradiated graphite was first suggested by Thrower [8] as an attempt to explain the vacancy line observed in TEM images of damaged graphite. The proposed configuration is analogous to that of azulene (**Fig. 1a**). This was, of course, before the breakthrough of nanoscience and nanotechnology and before the discovery of fullerenes and carbon nanotubes. This innovative concept had thus been overlooked for many

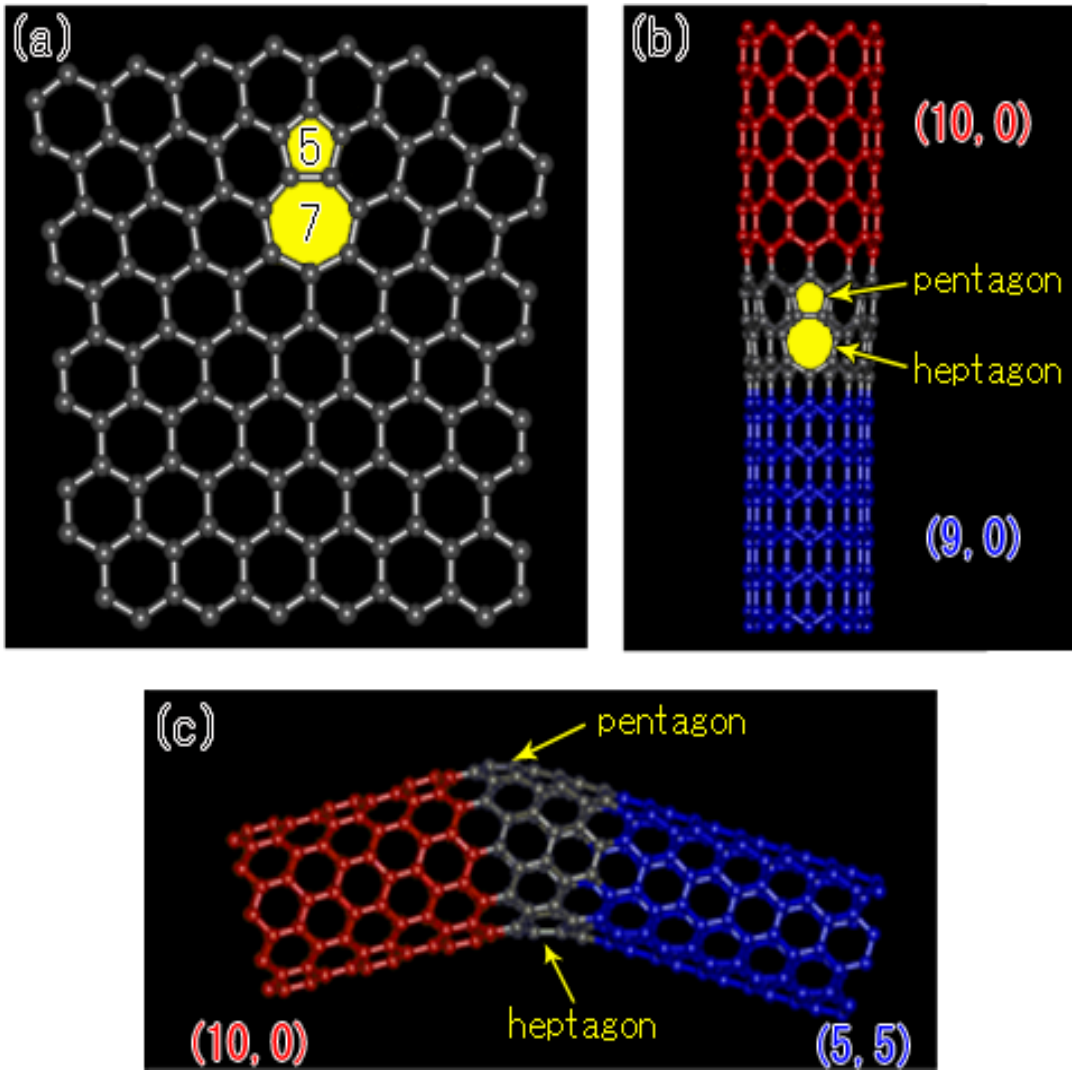

Fig. 1- (Color online) (a) A 5-7 pair in the hexagonal lattice, which was first proposed by Thrower [8]. (b) A (10, 0)-(9,0) SWCNT seamlessly connected through the 5-7 pair. (c) A bent SWCNT created through one pentagon and heptagon in the hexagonal lattice.

years.

More recently, the concept of the 5-7 pair has played an important role in the evolution of our understanding of diverse geometries in SWCNTs. It is well known that the hexagonal graphene sheet can be rolled up, forming a carbon nanotube. A rolled graphene structure with a 5-7 pair results in a SWCNT consisting of two SWCNTs segments having different tube diameters seamlessly connected through the 5-7 pair (**Fig. 1b**). Another example of such seamlessly connected SWCNTs is depicted in **Fig. 1c**; the SWCNT is bent at pentagon and heptagon sites, which are not required to be adjacent to each other. It is worthwhile to note that semiconducting and metallic SWCNTs can be seamlessly connected through such topological defects. Indeed, extending such geometries to construct new, more complex carbon nanostructures suggests itself as a very promising path to future carbon science, with a wealth of novel physicochemical properties.

2.2 Stone-Wales transformation and its extension to STW defects

Soon after the discovery of fullerenes, Stone and Wales proposed that many types of isomers of C_{60} can be generated by rotating a C-C bond between the two pentagons [9]. This structural rearrangement is called a Stone-Wales transformation (**Fig. 2a**).

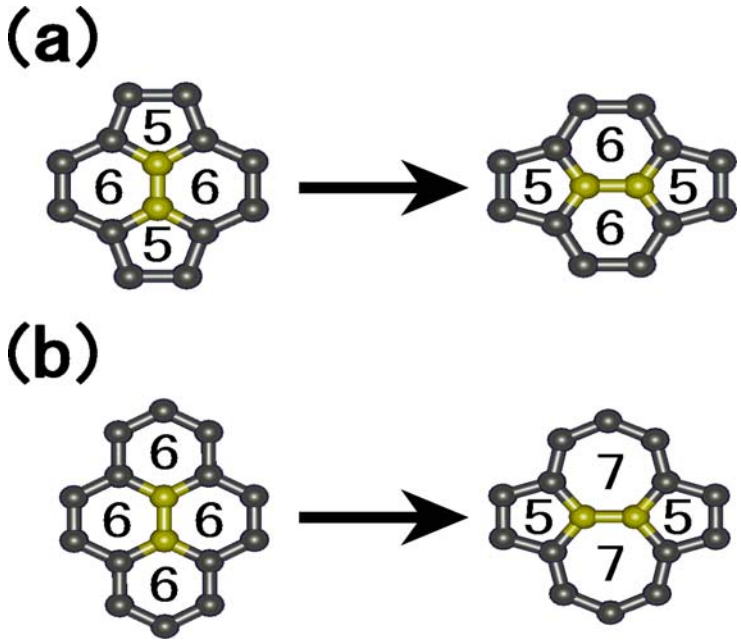

Fig. 2- (Color online) Schematics of (a) the Stone-Wales transformation and (b) the Thrower-Stone-Wales defect created through the 90° C-C bond rotation from four hexagons.

Extending the Stone-Wales transformation to the hexagonal lattice, two adjacent pentagon-heptagon pairs are obtained (**Fig. 2b**). The configuration shown in **Fig. 2b** had been referred to as the Stone-Wales defect. Since Thrower was the first to envisage the presence of a 5-7 defect in graphite, the term has been modified, and recently, referred to as the Stone-Thrower-Wales (STW) defect.

2.3 Experimental evidence of the STW defect

An atomic configuration similar to the STW defect can be found in dicyclopenta[*ef,kl*]heptalene (azupyrene), whose molecule consists of two 5-7 pairs terminated with hydrogens [17]. Azupyrene is a stable molecule that preserves planar structure. The STW defect should thus be energetically stable once generated in the hexagonal lattice; indeed, its presence in SWCNT and graphene is evidenced by direct HR-TEM observations, revealing dynamic creation, propagation, and annihilation of topological defects in the hexagonal lattice during electron irradiation [10,11]. An early SERS study has also verified the dynamic behavior of the STW defect in single-wall carbon nanohorns (SWCNH) [18], implying that the atomic rearrangements in the STW defect occur due to a strong electric field enhancement in the vicinity of SERS-active nanostructured metals. The presence of STW defects incorporated in SWCNHs is also

confirmed by a pulsed neutron diffraction method [19].

3. Dynamic nature of the STW defect as revealed by SERS

Fig. 3a shows a SERS spectrum probed in a single SWCNT detection and a regular Raman spectrum of the SWCNTs. The SWCNT sample (average diameter 1.37±0.25 nm) was produced by the laser ablation method [20] and used after acid purification. Both spectra were recorded with 532 nm excitation. Experimental details are shown elsewhere [21]. Briefly, droplets of SWCNTs dispersed in trichloroethylene were first deposited on a SERS-active silver foil, in order to obtain SERS spectra from a single SWCNT. Evaporation of the remaining trichloroethylene was then accomplished by heating at 423 K under 2 mPa using an in situ Raman cell. The SERS experiments were carried out under vacuum at ambient temperature. The spectrum collection time was 10 s. It is obvious that the SERS spectrum contains much more information than a regular Raman spectrum, which is enhanced by resonance Raman effects. The initial interpretation of SERS signals should include the vibrational modes of ideal SWCNTs [22-24] or graphite included in the material as impurities [25], before considering the vibrational modes of the STW defect.

The first-order Raman spectra of SWCNTs have been used extensively for characterization purposes, with a few observable signals such as low frequency radial

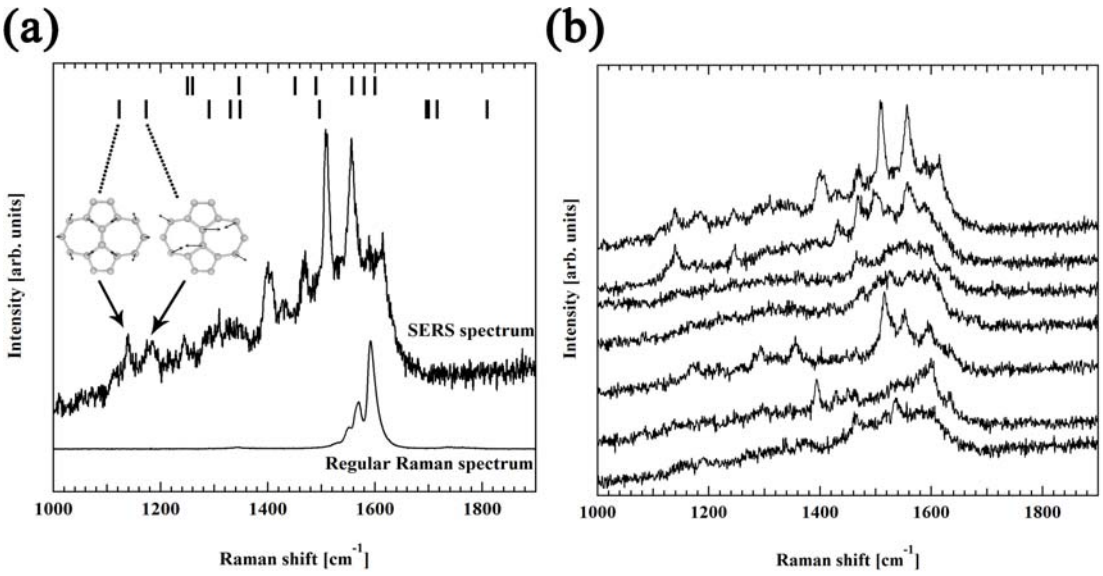

Fig. 3- (a) A SERS spectrum of a SWCNT and a regular Raman spectrum recorded from the bulk samples. Both spectra were obtained by 532 nm excitation. The calculated frequencies for graphite predicted by the double-resonance theory [25] and the STW defect in graphene (scaled by a factor of 0.9943 [28]) are shown by the upper and lower bars, respectively. Assigned vibrational modes of the STW defect are depicted in the inset. (b) A time sequence of SERS spectra of a SWCNT recorded from bottom to top at the same probing position.

breathing modes, disorder-induced D-bands, and multi-featured G-bands. Some predicted modes are still ambiguous in experiments. Since selection rules can be disrupted near the silver surface, resulting in observation of weak Raman modes or even IR-active modes [26], we compared the obtained SERS spectra not only with the regular Raman spectra but with predicted Raman- and IR-active frequencies [22]. Here, armchair SWCNTs, which are all classified as metallic SWCNTs, are excluded because the SWCNTs used in this study are in resonance with semiconducting SWCNTs by 532 nm excitation [27]. We also take into account the first-order vibrational modes of graphite, which are predicted by the double-resonance theory [25]. The theory predicts frequency dispersion of graphite modes associated with the excitation energy of incident light. Among the calculated vibrational modes of semiconducting SWCNTs and graphite (the vibrational frequencies calculated with 2.33 eV excitation are shown in Fig. 3a as bars), those vibrational modes are likely ruled out in the frequency range 1100-1200 cm^{-1} where the SERS spectrum shows explicit peaks.

Since SERS spectra show temporal fluctuations of frequencies and intensities (**Fig. 3b**), a phenomenon ascribed to the dynamic migration of topological defects during TEM observations [10,11], we expect that the SERS peaks at 1139 and 1183 cm^{-1} stem from the vibrational modes of the STW defect. According to frequency calculations of

the STW defect in a flat graphene model [28], two characteristic modes at 1122 and 1173 cm^{-1} are predicted within the frequency range concerned here. (These frequencies are normalized by factor of 0.9943 to reproduce the G-band frequency at 1582 cm^{-1}.) The predicted frequencies are depicted in **Fig. 3a** as bars and the corresponding atomic motions in the inset of **Fig. 3a**. The obtained SERS peaks at 1139 and 1183 cm^{-1} show good accordance with the calculated frequencies (at 1122 and 1173 cm^{-1}, respectively), indicating explicit SERS evidence for the presence of a TSW defect. Slight discrepancy between experiment and calculation (performed for the flat model) is attributed to frequency shifts induced by SWCNT curvature; an upshift of 9 cm^{-1} is expected for (10,10) SWCNT [29], whose diameter is close to the SWCNT used here.

4. Theoretical analysis of STW defects

4.1 Orientation of STW defect with respect to SWCNT axis

A fully localized vibrational mode in the C-C bond centered at the STW defect is another characteristic mode for the STW defect (**Fig. 4a**). Its frequency is predicted at 1810 cm^{-1} in the flat graphene model. According to DFT calculations by Miyamoto et al. [13], the frequency strongly depends on orientations of the C-C bond with respect to the tube axis for the SWCNT models. This mode predicted at 1810 cm^{-1} is not observed in

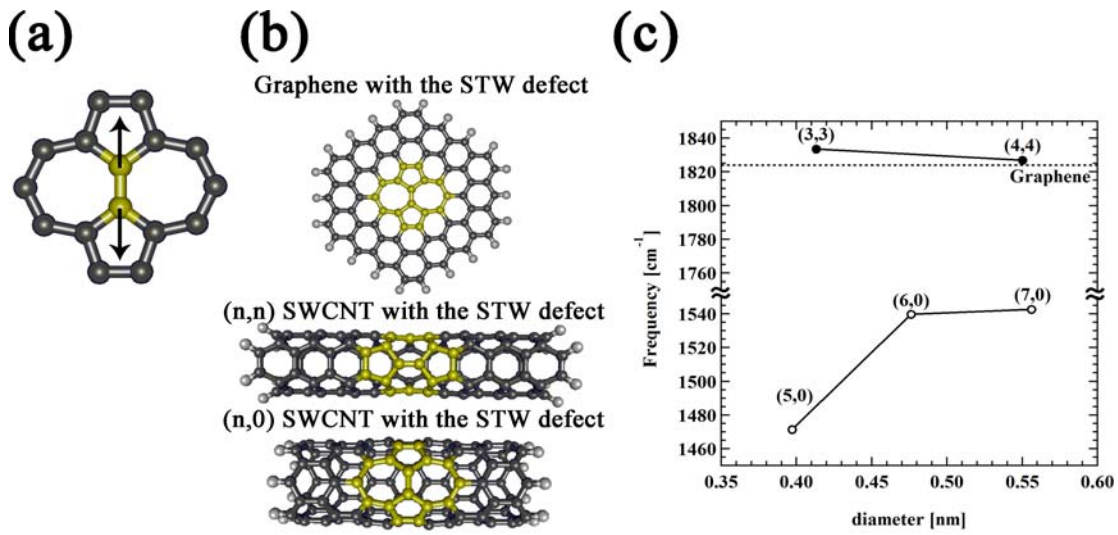

Fig. 4- (Color online) (a) A vibrational stretching mode localized in the center of the C-C bond of the STW defect. (b) Model structures used for DFT calculations at the B3LYP/6-31G level. Edges are terminated with hydrogen atoms. (c) Diameter dependence of the vibrational frequency depicted in (a). Filled and open circles correspond to (n,n) and (n,0) SWCNTs, respectively.

the SERS spectra, suggesting that the C-C bond of the STW defect is indeed tilted.

In support of this assumption, we performed DFT calculations using the Gaussian 09 software package [30] for model structures depicted in **Fig. 4b**. Geometry optimization and subsequent vibrational frequency calculations were carried out at the B3LYP level using the 6-31G basis set. Models of achiral SWCNTs with STW defects, generated by C-C bond rotation by 90°, are shown in Fig. 4b; the orientation of the C-C bond in an STW defect is parallel to the tube axis in an (n,n) armchair nanotube and normal to the tube axis in an (n,0) zigzag nanotube. Our frequency calculations, shown in **Fig. 4c,** agree with our expectation that the bond vibration is sensitive to the orientation of the C-C bond. While the frequencies for the (n,n) armchair SWCNTs (parallel configuration) show slight upshifts from that of graphene with the STW defect, which are nearly independent of tube diameters, the frequencies for the (n,0) zigzag SWCNTs (perpendicular configuration) are significantly lower from those for the parallel configurations. Furthermore, we can deduce from the trends shown in **Fig. 4c** that the frequency in the perpendicular configuration depends on the tube diameter in a very narrow range, and likely converges to ~1540 cm^{-1} as the diameter increases. We expect the above relations to be analogous to the frequency dependence of the two characteristic G-bands observed in Raman spectra of SWCNTs, such as the practically

diameter-independent G^+-band and the diameter-dependent G^--band, whose atomic motions are respectively, in the parallel and circumferential directions with respect to the tube axis [31]. Consequently, we conclude that the C-C bond signature of the STW defect observed in **Fig. 3a** should be interpreted as a tilt with respect to the tube axis, and that the SERS technique allows us to determine the STW defect orientation.

4.2 Stability of STW defects in flat and curved graphene structures

A practically significant example of the importance of orientation of the STW defect is the relative reactivity of the armchair vs. zigzag edge [32, 33]. This is illustrated in **Fig. 5**. When the C-C bond is parallel to the nanotube axis, the nanotube has a zigzag edge; when it is perpendicular to the tube axis, it has an armchair edge. We compared their oxidation reactivities by analyzing O_2 chemisorption, a process which culminates with desorption of CO from the armchair reactive site pair and CO_2 from the zigzag edge reactive site. We used DFT as implemented in the Gaussian 09 software [30], at the B3LYP/3-21G* level; comparison with representative results using a larger basis set, 6-31G(d), resulted in very similar trends. **Table 1** summarizes the results of thermochemical calculations. The numbers in parentheses for the zigzag structures correspond to the oxidation process that includes nascent site deactivation [34], i.e.,

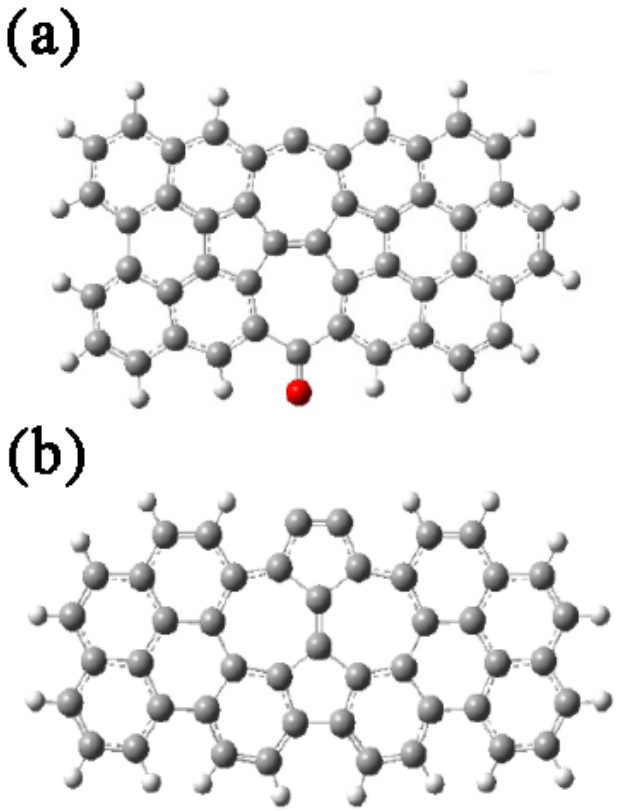

Fig. 5- (Color online) Optimized geometries of graphenes $C_{46}H_{16}O$ (a) and $C_{48}H_{18}$ (b). Their rolling produces, respectively, the zigzag SWCNT $C_{48}H_{10}O$ with a carbene-type reactive site and the armchair SWCNT $C_{48}H_{14}$ with a carbyne-type reactive site.

Table 1- Changes of the Helmoltz free energy, ΔH, and Gibbs free energy, ΔG, for the global process of carbon oxidation: Adsorption of O_2 on graphene (G) and its parent SWCNT followed by desorption of CO (from armchair structures) or CO_2 (from zigzag structures).

	ΔH (kcal/mol)	ΔG (kcal/mol)
ZZ-G (M=3)	-35.0 (-118)	-22.2 (-111)
ZZ-G+STW (M=3)	-50.0 (-133)	-45.5 (-127)
ZZ-SWCNT (M=1)	-74.5 (-122)	-69.3 (-115)
ZZ-SWCNT+STW (M=3)	-75.1 (-128)	-67.3 (-120)
AC-G (M=1)	-2.88	-8.20
AC-G+STW (M=1)	-61.5	-64.5
AC-SWCNT (M=1)	-33.6	-40.3
AC-SWCNT+STW (M=3)	-69.7	-74.1

M=Spin multiplicity of the ground state.

ZZ=Zigzag.

AC=Armchair.

conversion of the heptagon to a pentagon subsequent to CO_2 desorption. In all cases the oxidation process is both exothermic and thermodynamically favorable, as expected. The spin pairing processes are seen to differ for zigzag vs. armchair structures; these and other important details, including the energy barriers for the elementary steps of adsorption, surface rearrangement and desorption, are discussed elsewhere [35]. Of greatest relevance here are the following predictions: (1) Introduction of a STW defect destabilizes both the graphene and the parent SWCNT, in agreement with both intuitive expectations and experimental findings. (2) The armchair SWCNT (as well as the armchair graphene) is destabilized to a much greater extent than the zigzag SWCNT. This further highlights the usefulness of an experimental technique such as SERS that can detect the presence and orientation of STW defects in ubiquitously defective carbon materials.

5. Concluding remarks

Topological imperfections including the STW defect, are now understand to be extremely important structural features in graphene and nanocarbon materials, determine the local atomic arrangements and potentially delocalized electronic property changes. It is thus required to develop experimental capabilities to probe such

physicochemical properties, which remain ambiguous in many cases. We demonstrated that SERS is a powerful tool to sensitively detect the STW defect. Fluctuations of the SERS spectra are ascribed to defect migrations induced by strongly enhanced electric fields near the SERS-active sites. This enables investigations of dynamic behavior of topological defects using SERS. As single-wall tubular nanospaces exhibit unusual super-high pressure compression [36], molecular motion suppression [37], quantum molecular sieving [38] and ion sieving effects [39], the use of SERS to study STW-defect-associated dynamics of nano-range graphene structures holds promise to further develop nanocarbon science and technology.

Acknowledgements

This work was supported by Exotic Nanocarbons, Japan Regional Innovation Strategy Program by the Excellence, JST. TF and KK thank Dr. K. Takahashi at the Institute of Research and Innovation (IRI) for providing the SWCNT sample. ABST and LRR thank the Chilean sponsor (Fondecyt-Chile project #1080334) for financial support.

References

[1] Mackay AL and Terrones H. Diamond from graphite. Nature 1991;352:762.

[2] Lenosky T, Gonze X, Teter M, Elser V. Energetics of negatively curved graphitic carbon. Nature 1992;355:333-5.

[3] Iijima S, Ichihashi T, Ando Y. Pentagons, heptagons and negative curvature in graphite microtubule growth. Nature 1992;356:776-8.

[4] Kroto HW, Heath JR, O'Brien SC, Curl RF, Smalley RE. C_{60}: Buckminsterfullerene. Nature 1985;318:162-3.

[5] Terrones H and Terrones M. Curved nanostructured materials. New J Phys 2003;5:126.1-37.

[6] Lambin Ph and Biro LP. Structural properties of Haeckelite nanotubes. New J Phys 2003;5:141.1-14.

[7] Yoon M, Han S, Kim G, Lee SB, Berber S, Osawa E, et al. Zipper mechanism of nanotube fusion: Theory and experiment. Phys Rev Lett 2004;92(7):075504-1-4.

[8] Thrower PA. The Study of defects in graphite by transmission electron microscopy. In: Walker Jr PL, editor. Chemistry and physics of carbon, vol. 5. New York: Marcel Dekker; 1969. P.217-320.

[9] Stone AJ and Wales DJ. Theoretical studies of icosahedral C_{60} and some related species. Chem Phys Lett 1986;128(5, 6):501-503.

[10] Suenaga K, Wakabayashi H, Koshino M, Sato Y, Urita K, Iijima S. Imaging active

topological defects in carbon nanotubes. Nat Nanotechnol 2007;2:358-60.

[11] Meyer JC, Kisielowski C, Erni R, Rossell MD, Crommie MF, Zettl A. Direct imaging of lattice atoms and topological defects in graphene membranes. Nano Lett 2008;8(11):3582-6.

[12] Buongiorno Nardelli M, Fattebert J-L, Orlikowski D, Roland C, Zhao Q, Bernholc J. Mechanical properties, defects and electronic behavior of carbon nanotubes. Carbon 2000;38:1703-11.

[13] Miyamoto Y, Rubio A, Berber S, Yoon M, Tomanek D. Spectroscopic characterization of Stone-Wales defects in nanotubes. Phys Rev B 2004;69:121413(R).

[14] Meng FY, Zhou LG, Shi S-Q, Yang R. Atomic adsorption of catalyst metals on Stone-Wales defects in carbon nanotubes. Carbon 2003;41:2023-5.

[15] Lu X, Chen Z, Schleyer PvR. Are Stone-Wales defect sites always more reactive than perfect sites in the sidewalls of single-wall carbon nanotubes? J Am Chem Soc 2005;127:20-1.

[16] Campion A and Kambhampati P. Surface-enhanced Raman scattering. Chem Soc Rev 1998;27:241-50.

[17] Anderson Jr AG, Masada GM, Montana AF. The synthesis of dicyclopenta[*ef,kl*]heptalene (azupyrene). I. Routes to

1,6,7,8,9,9a-hexahydro-2*H*-benzo[*c*,*d*]azulen-6-one. J Org Chem 1973;38(8):1439-44.

[18] Fujimori T, Urita K, Aoki Y, Kanoh H, Ohba T, Yudasaka M, et al. Fine nanostructure analysis of single-wall carbon nanohorns by surface-enhanced Raman scattering. J Phys Chem C 2008;112(20): 7552-6.

[19] Hawelek L, Wrzalik W, Brodka A, Dore JC, Hannon AC, Iijima S, et al. A pulsed neutron diffraction study of the topological defects presence in carbon nanohorns. Chem Phys Lett 2011;502:87-91.

[20] Yudasaka M, Kokai F, Takahashi K, Yamada R, Sensui N, Ichihashi T, et al. J Phys Chem B 1999;163:3576.

[21] Fujimori T, Urita K, Ohba T, Kanoh H, Kaneko K. Evidence of dynamic pentagon-heptagon pairs in single-wall carbon nanotubes using surface-enhanced Raman scattering. J Am Chem Soc 2010;132(19):6764-7.

[22] Eklund PC, Holden JM, Jishi RA. Vibrational modes of carbon nanotubes; spectroscopy and theory. Carbon 1995;33(7):959-72.

[23] Saito R, Takeya T, Kimura T, Dresselhaus G, Dresselhaus MS. Raman intensity of single-wall carbon nanotubes. Phys Rev B 1998;57(7):4145-53.

[24] Ye L-H, Liu B-G, Wang D-S, Han R. Ab initio phonon dispersions of single-wall carbon nanotubes. Phys Rev B 2004;69:235409-1-10.

[25] Saito R, Jorio A, Souza Filho AG, Grueneis A, Pimenta MA, Dresselhaus G, et al. Dispersive Raman spectra observed in graphite and single wall carbon nanotubes. Physica B 2002;323:100-6.

[26] Ayars EJ, Hallen HD, Jahncke CL. Electric field gradient effects in Raman spectroscopy. Phys Rev Lett 2000;85(19):4180-3.

[27] Kataura H, Kumazawa Y, Maniwa Y, Umezu I, Suzuki S, Ohtsuka Y, et al. Optical properties of single-wall carbon nanotubes. Synth Met1999;103:2555-8.

[28] Wu G and Dong J. Raman characteristic peaks induced by the topological defects of carbon nanotube intramolecular junctions. Phy Rev B 2006;73:245414-1-9.

[29] Vandescuren M, Amara H, Langlet R, Lambin Ph. Characterization of single-walled carbon nanotubes containing defects from their local vibrational density of states. Carbon 2007;45:349-56.

[30] Frisch MJ, Trucks GW, Schlegel HB, Scuseria GE, Robb MA, Cheeseman JR, et al. Gaussian 09, Revision A.02, Gaussian, Inc., Wallingford CT (2009).

[31] Jorio A, Pimenta MA, Souza Filho AG, Saito R, Dresselhaus G, Dresselhaus MS. Characterizing carbon nanotube samples with resonance Raman scattering. New J Phys 2003;5:139.1-17.

[32] Radovic LR and Bockrath B. On the chemical nature of graphene edges: Origin of

stability and potential for magnetism in carbon materials. J Am Chem Soc 2005;127:5917-27.

[33] Radovic LR. Active sites in graphene and the mechanism of CO_2 formation in carbon oxidation. J. Am. Chem. Soc. 2009;131(47):17166-75.

[34] Radovic LR, Silva-Villalobos AF, Silva-Tapia AB, Vallejos-Burgos F. On the mechanism of nascent site deactivation in graphene. Carbon 2011;49:3471-87.

[35] Silva-Tapia AB. MS Thesis, University of Concepción, Chile, 2011.

[36] Urita K, Shiga Y, Fujimori T, Iiyama T, Hattori Y, Kanoh H, et al. Confinement in carbon nanospace-induced production of KI nanocrystals of high-pressure phase. J Am Chem Soc 2011;133:10344-7.

[37] Hashimoto S, Fujimori T, Tanaka H, Urita K, Ohba T, Kanoh H, et al. Anomaly of CH_4 molecular assembly confined in single-wall carbon nanohorn spaces. J Am Chem Soc 2011;133:2022-4.

[38] Noguchi D, Tanaka H, Fujimori T, Kagita H, Hattori Y, Honda H, et al. Selective D_2 adsorption enhanced by the quantum sieving effect on entangled single-wall carbon nanotubes. J Phys: Condens Matter 2010;22:334207(14pp).

[39] Yang C-M, Kim Y-J, Endo M, Kanoh H, Yudasaka M, Iijima S, et al. Nanowindow-regulated specific capacitance of supercapacitor electrodes of single-wall

carbon nanohorns. J Am Chem Soc 2006;129:20-1.

List of captions for figures and tables

Fig. 1- (Color online) (a) A 5-7 pair in the hexagonal lattice, which was first proposed by Thrower [8]. (b) A (10, 0)-(9,0) SWCNT seamlessly connected through the 5-7 pair. (c) A bent SWCNT created through one pentagon and heptagon in the hexagonal lattice.

Fig. 2- (Color online) Schematics of (a) the Stone-Wales transformation and (b) the Stone-Thrower-Wales defect created through the 90° C-C bond rotation from four hexagons.

Fig. 3- (a) A SERS spectrum of a SWCNT and a regular Raman spectrum recorded from the bulk samples. Both spectra were obtained by 532 nm excitation. The calculated frequencies for graphite predicted by the double-resonance theory [25] and the STW defect in graphene (scaled by a factor of 0.9943 [28]) are shown by the upper and lower bars, respectively. Assigned vibrational modes of the STW defect are depicted in the inset. (b) A time sequence of SERS spectra of a SWCNT recorded from bottom to top at the same probing position.

Fig. 4- (Color online) (a) A vibrational stretching mode localized in the center of the C-C bond of the STW defect. (b) Model structures used for DFT calculations at the B3LYP/6-31G level. Edges are terminated with hydrogen atoms. (c) Diameter dependence of the vibrational frequency depicted in (a). Filled and open circles correspond to (n,n) and (n,0) SWCNTs, respectively.

Fig. 5- (Color online) Optimized geometries of graphenes $C_{46}H_{16}O$ (a) and $C_{48}H_{18}$ (b). Their rolling produces, respectively, the zigzag SWCNT $C_{48}H_{10}O$ with a carbene-type reactive site and the armchair SWCNT $C_{48}H_{14}$ with a carbyne-type reactive site.

Table 1- Changes of the Helmoltz free energy, ΔH and Gibbs free energy, ΔG for the global process of carbon oxidation: Adsorption of O_2 on graphene (G) and its parent SWCNT followed by desorption of CO (from armchair structures) or CO_2 (from zigzag structures).